Catalytic asymmetric addition of Grignard reagents to alkenyl-substituted aromatic N-heterocycles

Jumde, Ravindra P.; Lanza, Francesco; Veenstra, Marieke J.; Harutyunyan, Syuzanna R.

Published in:
Science

DOI:
10.1126/science.aaf1983

Publication date:
2016

temporal resolution of the terahertz-driven streak camera could also be used to characterize electron microbunching in free-electron lasers, supplementing terahertz-based diagnostics for the x-ray output (*39*, *40*). The demonstrated concept is scalable to higher terahertz frequencies and multiple stages, offering the potential for cascaded compression into the subfemtosecond regime or direct injection into a single optical cycle of a laser-field accelerator (*12*). This may, in the long run, lead to isolated attosecond electron pulses for recording dynamic changes of electron distribution in complex systems, including biological molecules and solid-state nanostructures.

REFERENCES AND NOTES

1. W. Ackermann *et al.*, *Nat. Photonics* **1**, 336–342 (2007).
2. P. Emma *et al.*, *Nat. Photonics* **4**, 641–647 (2010).
3. G. H. Kassier *et al.*, *Rev. Sci. Instrum.* **81**, 105103 (2010).
4. C. M. Scoby, R. K. Li, E. Threlkeld, H. To, P. Musumeci, *Appl. Phys. Lett.* **102**, 023506 (2013).
5. C. Kealhofer *et al.*, *Opt. Lett.* **40**, 260–263 (2015).
6. D. J. Flannigan, A. H. Zewail, *Acc. Chem. Res.* **45**, 1828–1839 (2012).
7. G. Sciaini, R. J. D. Miller, *Rep. Prog. Phys.* **74**, 096101 (2011).
8. J. Tenboer *et al.*, *Science* **346**, 1242–1246 (2014).
9. M. Walbran, A. Gliserin, K. Jung, J. Kim, P. Baum, *Phys. Rev. Appl.* **4**, 044013 (2015).
10. S. Schulz *et al.*, *Nat. Commun.* **6**, 5938 (2015).
11. G. J. H. Brussaard *et al.*, *Appl. Phys. Lett.* **103**, 141105 (2013).
12. R. J. England *et al.*, *Rev. Mod. Phys.* **86**, 1337–1389 (2014).
13. E. Hemsing, G. Stupakov, D. Xiang, A. Zholents, *Rev. Mod. Phys.* **86**, 897–941 (2014).
14. E. Esarey, C. B. Schroeder, W. P. Leemans, *Rev. Mod. Phys.* **81**, 1229–1285 (2009).
15. M. C. Hoffmann, J. A. Fülöp, *J. Phys. D Appl. Phys.* **44**, 083001 (2011).
16. M. Shalaby, C. P. Hauri, *Nat. Commun.* **6**, 5976 (2015).
17. S. D. Vartak, N. M. Lawandy, *Opt. Commun.* **120**, 184–188 (1995).
18. R. B. Yoder, J. B. Rosenzweig, *Phys. Rev. ST Accel. Beams* **8**, 111301 (2005).
19. L. J. Wong, A. Fallahi, F. X. Kärtner, *Opt. Express* **21**, 9792–9806 (2013).
20. J. Fabiańska, G. Kassier, T. Feurer, *Sci. Rep.* **4**, 5645 (2014).
21. S. R. Greig, A. Y. Elezzabi, *Appl. Phys. Lett.* **105**, 241115 (2014).
22. L. Wimmer *et al.*, *Nat. Phys.* **10**, 432–436 (2014).
23. E. A. Nanni *et al.*, *Nat. Commun.* **6**, 8486 (2015).
24. Materials and methods are available as supplementary materials on *Science* Online.
25. W. Schneider *et al.*, *Opt. Lett.* **39**, 6604–6607 (2014).
26. F. J. García de Abajo, M. Kociak, *New J. Phys.* **10**, 073035 (2008).
27. E. Fill, L. Veisz, A. Apolonski, F. Krausz, *New J. Phys.* **8**, 272 (2006).
28. A. Gliserin, M. Walbran, F. Krausz, P. Baum, *Nat. Commun.* **6**, 8723 (2015).
29. F. O. Kirchner, A. Gliserin, F. Krausz, P. Baum, *Nat. Photonics* **8**, 52–57 (2014).
30. R. Kienberger *et al.*, *Nature* **427**, 817–821 (2004).
31. P. Baum, A. H. Zewail, *Proc. Natl. Acad. Sci. U.S.A.* **104**, 18409–18414 (2007).
32. A. Feist *et al.*, *Nature* **521**, 200–203 (2015).
33. General Particle Tracer code (www.pulsar.nl/gpt) .
34. J. Hoffrogge *et al.*, *J. Appl. Phys.* **115**, 094506 (2014).
35. V. S. Yakovlev, M. I. Stockman, F. Krausz, P. Baum, *Sci. Rep.* **5**, 14581 (2015).
36. H. C. Shao, A. F. Starace, *Phys. Rev. Lett.* **105**, 263201 (2010).
37. T. Plettner *et al.*, *Phys. Rev. Lett.* **95**, 134801 (2005).
38. S. Lahme, C. Kealhofer, F. Krausz, P. Baum, *Struct. Dyn.* **1**, 034303 (2014).
39. U. Frühling *et al.*, *Nat. Photonics* **3**, 523 (2009).
40. I. Grguraš *et al.*, *Nat. Photonics* **6**, 852 (2012).

ACKNOWLEDGMENTS

This work was supported by the European Research Council and the Munich-Centre for Advanced Photonics. We thank D. Frischke for preparing ultrathin aluminum foils. The authors declare no competing financial interests.

SUPPLEMENTARY MATERIALS

www.sciencemag.org/content/352/6284/429/suppl/DC1
Materials and Methods
Fig. S1
References (*41*–*43*)

4 December 2015; accepted 2 March 2016
10.1126/science.aae0003

REPORTS

ORGANIC CHEMISTRY

Catalytic asymmetric addition of Grignard reagents to alkenyl-substituted aromatic *N*-heterocycles

Ravindra P. Jumde, Francesco Lanza, Marieke J. Veenstra, Syuzanna R. Harutyunyan*

Catalytic asymmetric conjugate addition reactions represent a powerful strategy to access chiral molecules in contemporary organic synthesis. However, their applicability to conjugated alkenyl-*N*-heteroaromatic compounds, of particular interest in medicinal chemistry, has lagged behind applications to other substrates. We report a highly enantioselective and chemoselective catalytic transformation of a wide range of β-substituted conjugated alkenyl-*N*-heteroaromatics to their corresponding chiral alkylated products. This operationally simple methodology can introduce linear, branched, and cyclic alkyl chains, as well as a phenyl group, at the β-carbon position. The key to this success was enhancement of the reactivity of alkenyl-heteroaromatic substrates via Lewis acid activation, in combination with the use of readily available and highly reactive Grignard reagents and a copper catalyst coordinated by a chiral chelating diphosphine ligand.

The majority (88%) of all known active pharmaceutical ingredients (APIs) contain functionalized heterocyclic aromatic rings with a preponderance of *N*-containing aromatic heterocycles (*1*). Furthermore, approximately half of all APIs are chiral (*1*). Because the two enantiomers of a chiral drug can exhibit markedly different bioactivity, any new chiral API must be produced as a single enantiomer. Catalytic asymmetric carbon-carbon (C-C) bond formation represents the most straightforward and atom-efficient strategy for the construction of organic chiral molecules (*2*–*4*). Organometallic reagents are used in a substantial fraction of the C-C bond–forming reactions used to construct API molecules (*5*–*7*). The conjugate addition of organometallic reagents to electron-deficient substrates (Michael acceptors) has proven to be a powerful method for creating new C-C bonds in a catalytic asymmetric manner for more than 20 years (*7*–*12*). In this context, the catalytic asymmetric addition of organometallics to conjugated alkenyl-heteroaromatic compounds represents an attractive strategy to access valuable chiral heterocyclic aromatic compounds in enantiopure form. Addition of carbon nucleophiles to conjugated vinyl-substituted heteroaromatic compounds, leading mainly to achiral molecules, is well known (*13*, *14*). In contrast, there are only a handful of reports of nucleophilic additions to β-substituted analogs, in particular when organometallics are considered.

An early attempt at such a catalytic asymmetric reaction, reported in 1998, was the nickel-catalyzed addition of Grignard reagents to substituted 4-(1-alkenyl)pyridines (*15*). Although the reaction did not appear to be ligand-accelerated and provided only 0 to 15% enantiomeric excess (ee), these results suggested that catalytic asymmetric versions of such transformations were feasible. It was not until 2010 that a highly enantioselective, Rh-catalyzed addition of an organometallic reagent to alkenyl-substituted heteroaromatic compounds—namely arylation with an arylboronic acid—was realized, furnishing a wide range of chiral products with high yields and enantioselectivities (*16*–*19*).

The limited number of reports on transition metal–catalyzed asymmetric conjugate addition of nucleophiles to β-substituted alkenyl-heteroaromatic compounds, restricted to precious metal–catalyzed arylations, is in striking contrast to the plethora of methodologies available for the catalytic asymmetric alkylations, arylations, alkynylations, and allylations of common Michael acceptors, activated by carbonyl, nitrile, sulfonyl, and nitro groups (*8*–*12*). The paucity of methodologies for the nucleophilic addition to β-substituted alkenyl-heteroaromatic compounds is rooted in the intrinsically lower reactivity of these compounds, due to the relatively weak activation from the heteroaromatic moiety (*13*, *14*). Furthermore, the numerous examples of nonasymmetric additions to vinyl-substituted heteroaromatic compounds indicate that the presence of a β-substituent decreases the reactivity further, presumably because of the steric hindrance it introduces.

We decided to explore the addition of Grignard reagents to β-substituted conjugated alkenyl-heteroaromatic compounds. Inexpensive and readily available Grignard reagents are some of the most commonly used organometallics in synthetic chemistry (*20*), especially in copper-catalyzed asymmetric conjugate addition to a variety of Michael acceptors (*9*–*12*). We reasoned

Stratingh Institute for Chemistry, 9747 AG Groningen, Netherlands.
***Corresponding author. Email: s.harutyunyan@rug.nl**

that the high reactivity of Grignard reagents might be able to overcome the low reactivity of the β-substituted alkenyl heteroaromatics, and thus provide a solution to this long-standing challenge.

Here, we report an operationally simple, chemoselective, and highly enantioselective transformation of a wide range of β-substituted conjugated alkenyl-heteroaromatics to their corresponding chiral products via a copper-catalyzed addition of Grignard reagents, promoted by Lewis acid. Initially, we examined the reactivity of 2-styrylbenzoxazole (**1a**) toward EtMgBr (Et, ethyl) to produce racemic product **2a** (Fig. 1 and table S1). In the presence of CuBr·SMe_2 (Me, methyl), full conversion was not achieved and a complex mixture resulted after 24 hours at −25°C, which confirms the markedly lower reactivity of β-substituted alkenyl-heteroaromatic substrates relative to typical Michael acceptors. Chiral ferrocenyl diphosphine ligand **L1** (Fig. 1A) did not improve the results.

The activation of electrophilic substrates toward nucleophilic addition is commonly achieved using Lewis acids (LAs) (*21*–*23*). We anticipated that LA activation of alkenyl-heteroaromatic substrates could be a viable strategy to overcome the reactivity issues. During our previous studies, focused on the synthesis of silyl-substituted chiral tertiary alcohols via addition of Grignard reagents to acyl silanes, we used LA mixtures to promote the addition over the reduction pathway (*24*). We also learned that LAs are compatible with both chiral copper catalysts and Grignard reagents, as long as reactions are carried out at temperatures below −50°C. Inspired by these findings, we set out to evaluate the effect of LA in the aforementioned reaction (table S1). To our surprise, no conversion of **1a** was observed when EtMgBr was used as nucleophile in toluene at −78°C, in the presence of CuBr·SMe_2 and BF_3·OEt_2 as LA. However, the addition of chiral ligand **L1** led to the desired product **2a** with 59% isolated yield and 87% enantioselectivity. The effect of different LAs on the activation of **1a** was studied next; $TiCl_4$, trimethylsilyl chloride (TMSCl), $MgBr_2$, and trimethylsilyl trifluoromethanesulfonate (TMSOTf) were examined, but none performed better than BF_3·OEt_2 (table S1).

Having established the optimal LA for the activation of **1a** toward EtMgBr, we assessed the effect of the chiral ligand and different solvents (Fig. 1A and table S1). Chiral ligand screening revealed the sterically hindered ferrocenyl ligand **L2**, as well as phosphoramidite-type ligands **L6** and **L7**, to be ineffective, while ferrocenyl ligand ***L3*** furnished product **2a** in a modest yield and

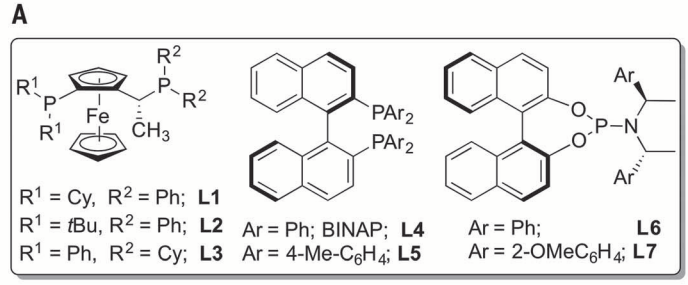

Fig. 1. Chiral ligands and heterocycle scope. (**A**) Structure of chiral ligands tested during the optimization studies. (**B**) Heterocycle scope. Reactions were conducted on a 0.2 mmol scale. Reported yields are for isolated products. Full conversion was obtained in all cases after 18 hours (isolated yields below 65% are due to the by-product derived from formal trapping of the product enolate by the substrate). Absolute configurations were assigned by analogy with the literature. *3 equiv of EtMgBr and 2.2 equiv of BF_3·OEt_2 were used in this case. †Using *t*BuOMe or toluene instead of diethyl ether provides the addition product **2m** with 92% and 80% isolated yields, respectively, and 99% ee.

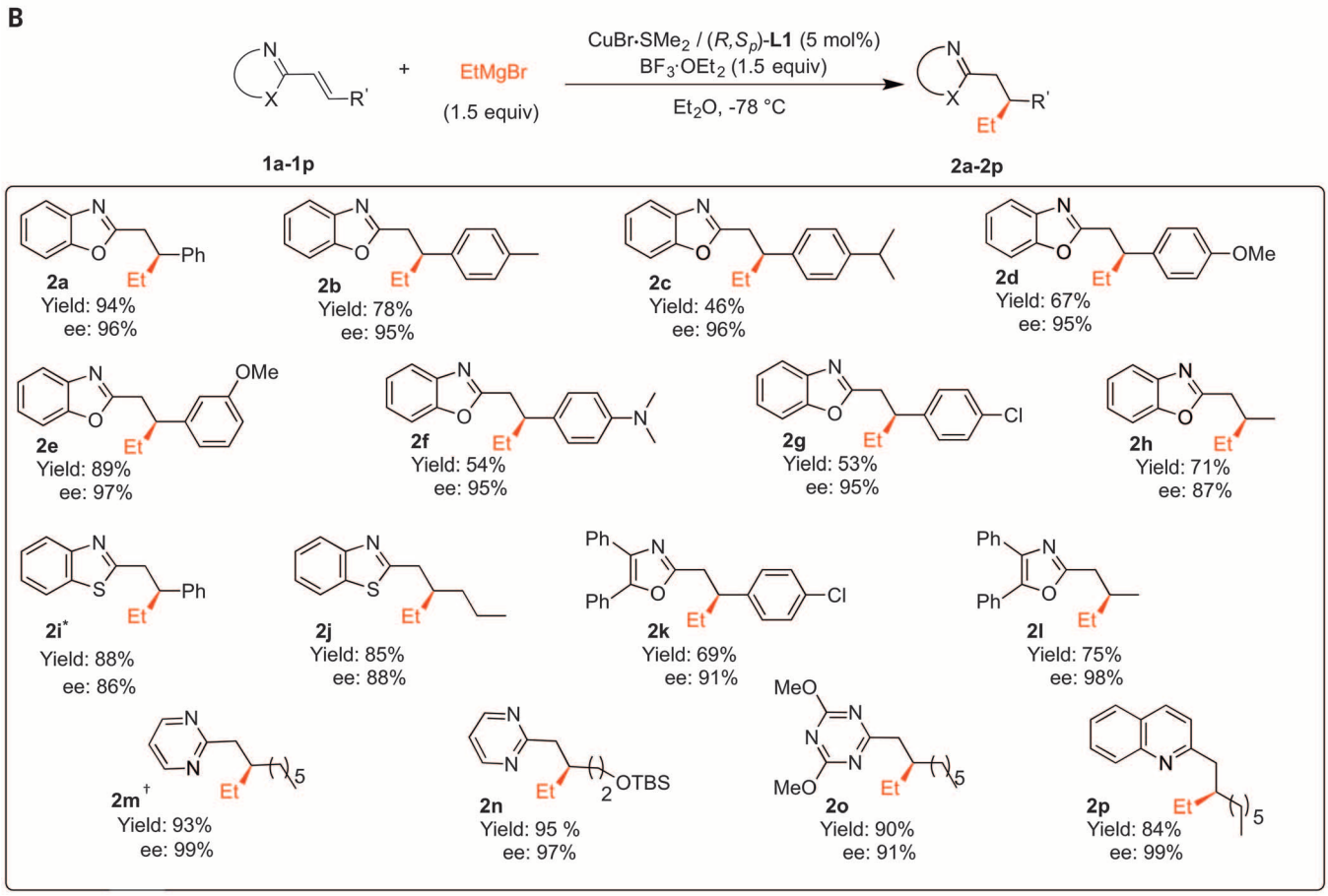

enantioselectivity. Both binaphthyl diphosphine–type ligand **L4** (BINAP) and ligand **L5** performed better, furnishing the addition product with >90% ee.

We concluded that several chiral diphosphine ligands, in combination with a Cu(I) salt, are capable of effectively addressing the reactivity of the substrate and the enantioselectivity of the reaction. However, the superior yield obtained with ferrocenyl ligand **L1** prompted us to select it as the optimal ligand. Therefore, we studied the effect of different solvents (table S1) using the catalytic system derived from $CuBr{\cdot}SMe_2$ and **L1**. With the exception of tetrahydrofuran, all solvents tested [Et_2O, *t*BuOMe (Bu, butyl), toluene, CH_2Cl_2] were effectively tolerated by the alkylation protocol, providing **2a** with excellent ee. The best results—excellent yield (94%) and enantioselectivity (96%)—were obtained in Et_2O. Thus, we adopted the following optimized reaction conditions for the remainder of our experiments: $CuBr{\cdot}SMe_2/(R,S_p)$-**L1** (5 mol %), Grignard reagent (1.5 equiv), $BF_3{\cdot}OEt_2$ (1.5 equiv), 18 hours of reaction time at –78°C in Et_2O solvent.

For the evaluation of the substrate scope, we chose the reaction between alkenyl-heteroaromatic substrates **1a** to **1p** and EtMgBr (Fig. 1B). To assess the stereoelectronic effects of the β-substituent on the reaction, we synthesized a range of substrates **1a** to **1h**, derived from benzoxazole, and subjected them to our alkylation protocol.

The enantioselectivity of the reaction was found to be consistently high for substrates bearing both electron-rich and electron-poor substituents. However, the reactivity of the substrate proved to be strongly dependent on the nature of these substituents, providing products **2a** to **2g** with a broad range of isolated yields and no clear trend. The addition of EtMgBr to benzoxazole **1h**, bearing an adjacent propenyl moiety, proceeded smoothly, furnishing the corresponding product **2h** in good yield and enantioselectivity. We also explored other heteroaromatic substrates, such as thiazoles (**1i** and **1j**), oxazoles (**1k** and **1l**), pyrimidines (**1m** and **1n**), triazines (**1o**), and quinoline (**1p**), and were pleased that our protocol was successful for all tested examples, furnishing the corresponding alkylated products with high yields and enantiopurities. This insensitivity to the presence of heteroatoms in the substrate, which might be expected to interfere with the stability of the chiral copper catalyst, makes the reaction remarkably general.

Next, we used two structurally different conjugated alkenyl-heteroaromatic compounds as

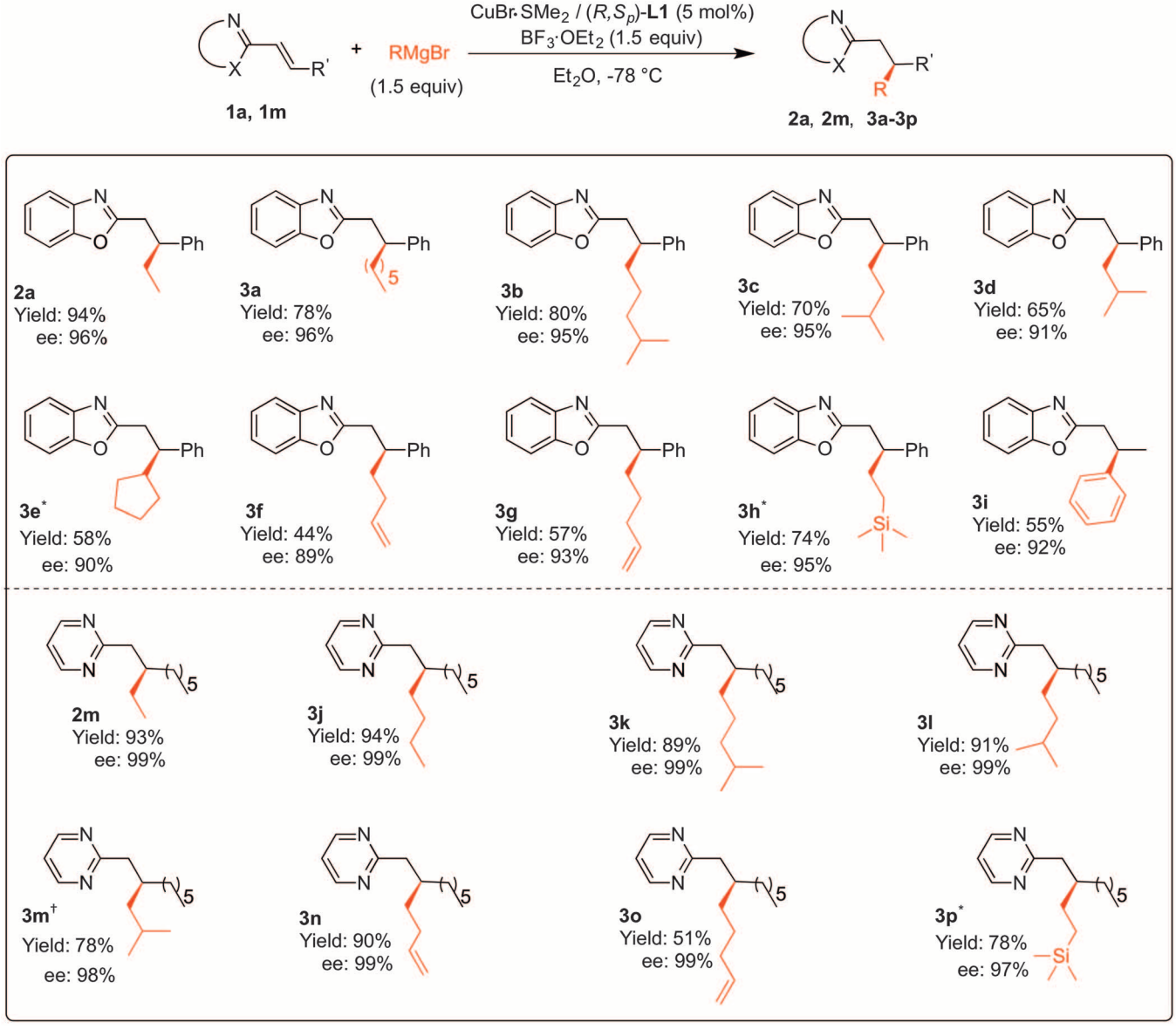

Fig. 2. Grignard scope. Reaction conditions were the same as specified in Fig. 1. *3 equiv of EtMgBr and 2 equiv of $BF_3{\cdot}OEt_2$ were used in this case. †Solvent mixture Et_2O/CH_2Cl_2 (2:1) was used in this case.

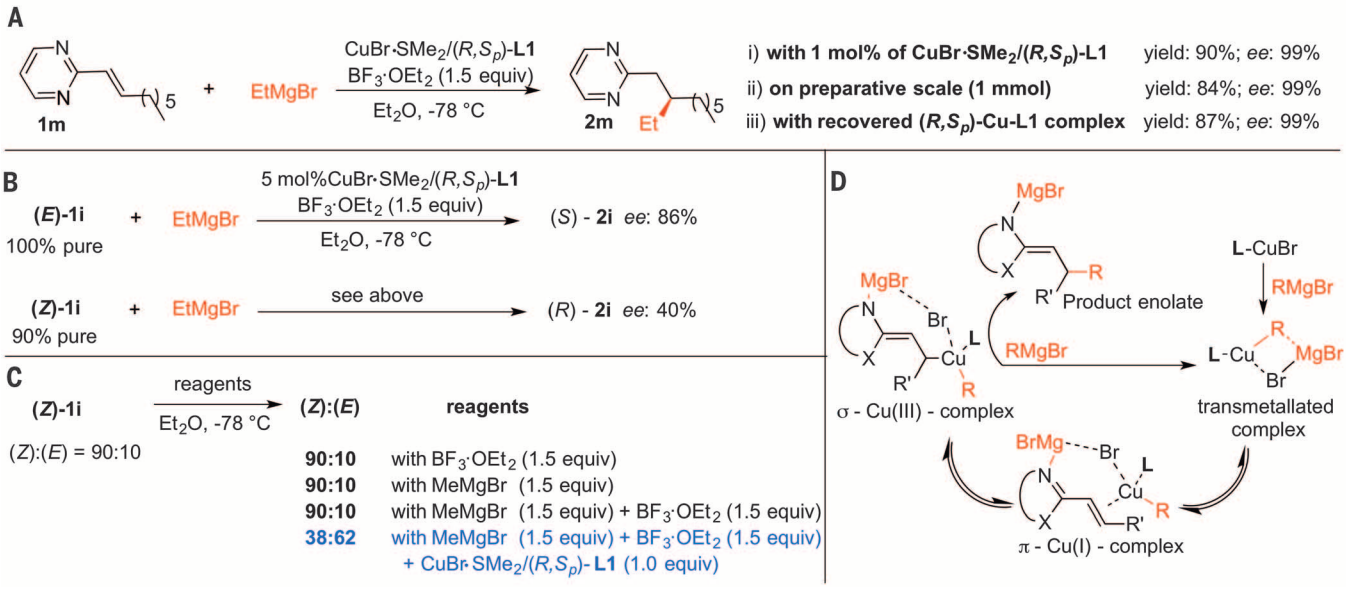

Fig. 3. Scale-up and mechanistic considerations. (**A**) Experiments (i) with 1 mol % of CuBr·SMe_2/(R,S_p)-**L1**, (ii) on a preparative scale, and (iii) with the recovered catalyst. (**B**) Catalytic asymmetric addition of EtMgBr to (*E*)-**1i** and (*Z*)-**1i**. (**C**) Studies on (*E*)/(*Z*) isomerization of **1i**. (**D**) Hypothetical catalytic cycle.

substrates—**1a** and **1m**, derived from benzoxazole and pyrimidine, respectively—to evaluate the scope of the nucleophile (Fig. 2). Nearly all Grignard reagents assessed provided excellent enantioselectivities. It was particularly gratifying that, where previous reports on additions to conjugated alkenyl-heteroaromatics were restricted to arylations, our catalytic system enabled the addition of a wide variety of alkyl Grignard reagents. Different chain lengths (Et, *n*-Bu, and *n*-hexyl) furnished the corresponding products (**2a**, **3a**, **2m**, and **3j**) with excellent enantioselectivities (96 to 99%). Sterically more demanding α-, β-, γ-, and δ-branched Grignard reagents were also well tolerated, providing the corresponding products (**3b** to **3e**; **3k** to **3m**) with enantioselectivities ranging from 90 to 99%.

The presence of an olefinic or trimethylsilyl moiety in the Grignard reagent was also tolerated, demonstrating that functionalized products (**3f** to **3h**; **3n** to **3p**) can be obtained in high enantiopurity as well, albeit with moderate yields in a few cases. Only for the least reactive Grignard reagent, MeMgBr, was no conversion of either substrate obtained. Although the enantioselective arylation by organoboron reagents is a well-established methodology for this type of substrate (*16*), we were curious as to whether our protocol could tolerate aryl nucleophiles as well. To our satisfaction, we observed that the same protocol supported the addition of a phenyl group, and product **3i** could be obtained with 92% enantioselectivity when PhMgBr was used as nucleophile. The addition of various Grignard reagents to the pyrimidine-derived substrate **1m** provided the corresponding products **2m** and **3j** to **3p** consistently with enantioselectivities above 97%. However, **1m** is more sensitive than other heteroaromatic substrates to steric hindrance. For instance, no conversion of **1m** was observed for the addition of *c*-pentyl-MgBr.

To examine the potential for the scaling up of these reactions, we performed a series of experiments for the addition of EtMgBr to substrate **1m**: (i) with 1 instead of 5 mol % of CuBr·SMe_2/(R,S_p)-**L1**, (ii) on a preparative scale (1 mmol), and (iii) with recovered catalyst in the form of the Cu complex of (R,S_p)-**L1** (Fig. 3A). In all three experiments, we were able to obtain the product **2m** with excellent yield and enantioselectivity, without any erosion from the original values.

All heteroaromatic substrates prepared in this work were obtained with more than 99% (*E*)-configurational purity. Because the geometry of the double bond is expected to have substantial influence on the stereoselectivity in asymmetric reactions involving alkene transformations, we studied the effect of the alkene geometry in the addition of EtMgBr to (*E*)- and (*Z*)-stereoisomers of 2-styrylbenzothiazole (**1i**). Upon ultraviolet light irradiation of (*E*)-**1i**, its stereoisomer, (*Z*)-**1i**, was obtained with 90% purity. The enantioselective addition of EtMgBr to both (*E*)-**1i** and (*Z*)-**1i**, catalyzed by the CuBr·SMe_2/(R,S_p)-**L1** catalyst, led to the addition product **2i** with opposite configuration and distinctly different enantioselectivities [40% ee for (*Z*)-**1i** and 86% ee for (*E*)-**1i**] (Fig. 3B). The lower enantioselectivity obtained when (*Z*)-**1i** was used as substrate can be explained by partial isomerization of the substrate during the reaction, caused by the active catalyst. Unfortunately, the high reaction rate of the catalytic addition of EtMgBr to (*Z*)-**1i** prevented the analysis of the reaction mixture at different times. Using MeMgBr, with which no conversion occurs, we found that isomerization indeed took place, but only when CuBr·SMe_2, (R,S_p)-**L1**, BF_3·OEt_2, and MeMgBr were all present in solution (Fig. 3C). This isomerization is similar to that observed in the Cu(I)-catalyzed conjugate addition of Grignard reagents to α,β-unsaturated esters (*25*). By analogy, this isomerization supports the catalytic cycle (Fig. 3D) involving transmetallation of the copper complex formed from CuBr·SMe_2 and **L1**, followed by reversible formation of the π-Cu(I) complex, the σ-Cu(III) complex, and finally, irreversible reductive elimination to form aza-enolate of **2i** (*25*, *26*).

The precise mechanism of this reaction remains under investigation, as the role of the LA additive is not clear. It seemed plausible for the LA to activate the heteroaromatic substrate toward the addition reaction. However, preliminary nuclear magnetic resonance (NMR) spectroscopic studies have revealed that new species are formed upon addition of BF_3·OEt_2 to each of the components of the reaction individually, indicating that the LA can modulate the reactivity of Grignard reagents and can also be involved in the structure of the catalytically active species.

REFERENCES AND NOTES

1. J. A. Blacker, M. T. Williams, Eds., *Pharmaceutical Process Development: Current Chemical and Engineering Challenges* (Royal Society of Chemistry, 2011).
2. E. N. Jacobsen, A. Pfaltz, H. Yamamoto, Eds., *Comprehensive Asymmetric Catalysis I–III* (Springer, 1999).
3. I. Ojima, Ed., *Catalytic Asymmetric Synthesis* (Wiley, ed. 3, 2010).
4. M. Gruttadauria, F. Giacalone, Eds., *Catalytic Methods in Asymmetric Synthesis: Advanced Materials, Techniques, and Applications* (Wiley, 2011).
5. V. Farina, J. T. Reeves, C. H. Senanayake, J. J. Song, *Chem. Rev.* **106**, 2734–2793 (2006).
6. G. G. Wu, F. X. Chen, K. Yong, in *Comprehensive Chirality*, E. M. Carreira, H. Yamamoto, Eds. (Elsevier, 2012), pp. 147–208.
7. G. P. Howell, *Org. Process Res. Dev.* **16**, 1258–1272 (2012).
8. T. Hayashi, K. Yamasaki, *Chem. Rev.* **103**, 2829–2844 (2003).
9. A. Alexakis, N. Krause, S. Woodward, Eds., *Copper-Catalyzed Asymmetric Synthesis* (Wiley-VCH, 2014).
10. S. R. Harutyunyan, T. den Hartog, K. Geurts, A. J. Minnaard, B. L. Feringa, *Chem. Rev.* **108**, 2824–2852 (2008).
11. A. Alexakis, J. E. Bäckvall, N. Krause, O. Pàmies, M. Diéguez, *Chem. Rev.* **108**, 2796–2823 (2008).
12. T. Jerphagnon, M. G. Pizzuti, A. J. Minnaard, B. L. Feringa, *Chem. Soc. Rev.* **38**, 1039–1075 (2009).
13. D. A. Klumpp, *Synlett* **23**, 1590–1604 (2012).

14. D. Best, H. W. Lam, *J. Org. Chem.* **79**, 831–845 (2014).
15. I. N. Houpis *et al.*, *Tetrahedron* **54**, 1185–1195 (1998).
16. G. Pattison, G. Piraux, H. W. Lam, *J. Am. Chem. Soc.* **132**, 14373–14375 (2010).
17. A. Saxena, H. W. Lam, *Chem. Sci.* **2**, 2326–2331 (2011).
18. L. Rupnicki, A. Saxena, H. W. Lam, *J. Am. Chem. Soc.* **131**, 10386–10387 (2009).
19. A. A. Friedman, J. Panteleev, J. Tsoung, V. Huynh, M. Lautens, *Angew. Chem. Int. Ed.* **52**, 9755–9758 (2013).
20. H. G. Richey, *Grignard Reagents: New Developments* (Wiley, 1999).
21. H. Yamamoto, Ed., *Lewis Acids in Organic Synthesis, Volume 1–2* (Wiley-VCH, 2000).
22. E. Marcantoni, M. Petrini, In *Lewis Acid Promoted Addition Reactions of Organometallic Compounds* (Elsevier, 2014), pp. 344–364.
23. Y. Yamamoto, S. Yamamoto, H. Yatagai, Y. Ishihara, K. Maruyama, *J. Org. Chem.* **47**, 119–126 (1982).
24. J. Rong, R. Oost, A. Desmarchelier, A. J. Minnaard, S. R. Harutyunyan, *Angew. Chem. Int. Ed.* **54**, 3038–3042 (2015).
25. S. R. Harutyunyan *et al.*, *J. Am. Chem. Soc.* **128**, 9103–9118 (2006).
26. N. Yoshikai, E. Nakamura, *Chem. Rev.* **112**, 2339–2372 (2012).

ACKNOWLEDGMENTS

Supported by Netherlands Organization for Scientific Research NWO-Vidi and ECHO grants (S.R.H.) and Ministry of Education, Culture and Science Gravity program grant 024.001.035 (S.R.H.). We thank J. T. A. de Jong, B. Maciá, and J. F. Collados for helpful comments on the manuscript.

SUPPLEMENTARY MATERIALS

www.sciencemag.org/content/352/6284/433/suppl/DC1
Materials and Methods
Table S1
NMR spectra
References (*27*–*35*)

6 January 2016; accepted 22 March 2016
10.1126/science.aaf1983

MAGNETISM

Atomic-scale control of graphene magnetism by using hydrogen atoms

Héctor González-Herrero,[1,2] José M. Gómez-Rodríguez,[1,2,3] Pierre Mallet,[4,5] Mohamed Moaied,[1,6] Juan José Palacios,[1,2,3] Carlos Salgado,[1] Miguel M. Ugeda,[7,8] Jean-Yves Veuillen,[4,5] Félix Yndurain,[1,2,3] Iván Brihuega[1,2,3]*

Isolated hydrogen atoms absorbed on graphene are predicted to induce magnetic moments. Here we demonstrate that the adsorption of a single hydrogen atom on graphene induces a magnetic moment characterized by a ~20–millielectron volt spin-split state at the Fermi energy. Our scanning tunneling microscopy (STM) experiments, complemented by first-principles calculations, show that such a spin-polarized state is essentially localized on the carbon sublattice opposite to the one where the hydrogen atom is chemisorbed. This atomically modulated spin texture, which extends several nanometers away from the hydrogen atom, drives the direct coupling between the magnetic moments at unusually long distances. By using the STM tip to manipulate hydrogen atoms with atomic precision, it is possible to tailor the magnetism of selected graphene regions.

Adding magnetism to the long list of graphene's capabilities has been pursued since this material was first isolated (*1*). From a theoretical point of view, magnetic moments in graphene can be induced by removing a single p_z orbital from the π-graphene system; this removal creates a single π-state at the Fermi energy (E_F) around the missing orbital. The double occupation of this state by two electrons with different spins is forbidden by the electrostatic Coulomb repulsion; namely, once an electron occupies the state, a second one with opposite spin needs to "pay" an extra energy U. This leaves a single electron occupying the state and therefore a net magnetic moment (*2*–*6*). The strength of U, which determines the spin splitting, depends on the spatial localization of the state, because this defines the proximity of the electrons (Fig. 1A). In contrast to magnetic moments of a strongly localized atomic character that are commonly found in magnetic materials, these induced moments are predicted to extend over several nanometers, suggesting a strong direct coupling between them at unusually long distances. The coupling rules between the induced magnetic moments are also expected to be simple. Because of the bipartite atomic structure of graphene—which consists of two equivalent triangular sublattices, labeled A and B—and according to Lieb's theorem (*7*), the ground state of the system possesses a total spin given by $S = 1/2 \times |N_A - N_B|$, where N_A and N_B are the number of p_z orbitals removed from each sublattice (*4*, *8*, *9*). Thus, to generate a net magnetic moment in a particular graphene region, a different number of p_z orbitals from each sublattice needs to be locally removed.

Many theoretical proposals have been put forward on this subject, involving zigzag edges, graphene clusters, grain boundaries, and atomic defects (*2*, *4*, *5*, *8*–*11*). Experimentally, the removal of p_z orbitals from the π system has been achieved by randomly creating atomic vacancies or adsorbing adatoms (*12*–*16*). However, removing those p_z orbitals in a controlled manner has turned out to be challenging. In this work, we relied on the simplest (albeit demanding) experimental approach to remove a single p_z orbital from the graphene network by means of the adsorption of a single H atom. Atomic H chemisorbs on graphene on top of carbon atoms, changing the initial sp^2 hybridization of carbon to essentially sp^3 (*17*, *18*) and effectively removing the corresponding p_z orbital (*4*, *19*, *20*). In this sense, chemisorbed H atoms are equivalent to carbon vacancies (*4*, *12*, *14*) but with the advantage that, unlike vacancies, they leave the graphene atomic lattice with no unsaturated dangling bonds, preserving the threefold symmetry. Our experiments, supported by ab initio calculations, provide a comprehensive picture of the origin, coupling, and manipulation of the magnetism induced by H atoms on graphene layers.

We deposited atomic H on graphene grown on a SiC(000-1) substrate (*21*). In this system, the rotational disorder of the graphene layers electronically decouples the π bands, leading to a stacking of essentially isolated graphene sheets (*22*–*24*). Scanning tunneling microscopy (STM) visualizes single H atoms as a bright protrusion (apparent height, ~2.5 Å) surrounded by a complex threefold √3×√3 pattern that is rotated 30° degrees with respect to the graphene lattice. (*25*, *26*) [Fig. 1B and section 1 in (*27*)]. The resolution that we achieved allowed us to identify the adsorbate as a single H atom and to determine the atomic site (and thus the corresponding atomic sublattice) where each H atom was chemisorbed by means of comparison with density functional theory (DFT)–simulated STM images [Fig. 1D and section 1 in (*27*)]. As depicted in Fig. 1A, graphene magnetic moments induced by H adsorption should be reflected in the appearance of a spin-polarized state at E_F, which, according to DFT calculations, should be characterized by two narrow peaks in the density of states (DOS) (Fig. 1E) (*4*).

Differential conductance spectra (dI/dV; I, current; V, sample voltage) probe the energy-resolved local DOS under the STM tip position and thus are ideal for investigating this question. Figure 1C shows two dI/dV spectra, measured at 5 K, that are representative of our findings. The dI/dV spectra measured on clean graphene, located far enough away from defects, have the characteristic featureless V shape of graphene, with a minimum at E_F indicating the position of

[1]Departamento de Física de la Materia Condensada, Universidad Autónoma de Madrid, E-28049 Madrid, Spain. [2]Condensed Matter Physics Center (IFIMAC), Universidad Autónoma de Madrid, E-28049 Madrid, Spain. [3]Instituto Nicolás Cabrera, Universidad Autónoma de Madrid, E-28049 Madrid, Spain. [4]Université Grenoble Alpes, Institut NEEL, F-38042 Grenoble, France. [5]Centre National de la Recherche Scientifique (CNRS), Institut NEEL, F-38042 Grenoble, France. [6]Department of Physics, Faculty of Science, Zagazig University, 44519 Zagazig, Egypt. [7]CIC nanoGUNE, 20018 Donostia-San Sebastian, Spain. [8]Ikerbasque, Basque Foundation for Science, 48013 Bilbao, Spain.
***Corresponding author. Email: ivan.brihuega@uam.es**

Catalytic asymmetric addition of Grignard reagents to alkenyl-substituted aromatic *N*-heterocycles

Ravindra P. Jumde, Francesco Lanza, Marieke J. Veenstra and Syuzanna R. Harutyunyan

Science **352** (6284), 433-437.
DOI: 10.1126/science.aaf1983

Copper adds alkyls asymmetrically

Nitrogen-bearing rings are very common features in the molecular structures of modern drugs. Reactions that can modify these N heterocycles selectively are thus especially useful to optimize pharmaceutical properties. Jumde *et al.* developed a method to append alkyl groups in a single mirror-image orientation to substituted C=C double bonds dangling from N heterocycles. The copper-catalyzed reaction, which relies on Grignard reagents to introduce the alkyl groups, manifests high selectivity across a broad range of substrates, with no interference from the nitrogen.

Science, this issue p. 433